A PDRMIP Multimodel Study on the Impacts of Regional Aerosol Forcings on Global and Regional Precipitation

L. Liu,[a,b] D. Shawki,[a] A. Voulgarakis,[a] M. Kasoar,[a] B. H. Samset,[c] G. Myhre,[c]
P. M. Forster,[d] Ø. Hodnebrog,[c] J. Sillmann,[c] S. G. Aalbergsjø,[c] O. Boucher,[e]
G. Faluvegi,[f] T. Iversen,[g] A. Kirkevåg,[g] J.-F. Lamarque,[h] D. Olivié,[g]
T. Richardson,[d] D. Shindell,[i] and T. Takemura[j]

[a] Department of Physics, Imperial College London, London, United Kingdom
[b] Northwest Institute of Nuclear Technology, Xi'an, China
[c] Center for International Climate and Environmental Research, Oslo, Norway
[d] University of Leeds, Leeds, United Kingdom
[e] Institut Pierre-Simon Laplace, Université Pierre et Marie Curie/CNRS, Paris, France
[f] NASA Goddard Institute for Space Studies, Columbia University, New York, New York
[g] Norwegian Meteorological Institute, Oslo, Norway
[h] NCAR/University Center for Atmospheric Research, Boulder, Colorado
[i] Duke University, Durham, North Carolina
[j] Kyushu University, Fukuoka, Japan

ABSTRACT

Atmospheric aerosols such as sulfate and black carbon (BC) generate inhomogeneous radiative forcing and can affect precipitation in distinct ways compared to greenhouse gases (GHGs). Their regional effects on the atmospheric energy budget and circulation can be important for understanding and predicting global and regional precipitation changes, which act on top of the background GHG-induced hydrological changes. Under the framework of the Precipitation Driver Response Model Intercomparison Project (PDRMIP), multiple models were used for the first time to simulate the influence of regional (Asian and European) sulfate and BC forcing on global and regional precipitation. The results show that, as in the case of global aerosol forcing, the global fast precipitation response to regional aerosol forcing scales with global atmospheric absorption, and the slow precipitation response scales with global surface temperature response. Asian sulfate aerosols appear to be a stronger driver of global temperature and precipitation change compared to European aerosols, but when the responses are normalized by unit radiative forcing or by aerosol burden change, the picture reverses, with European aerosols being more efficient in driving global change. The global apparent hydrological sensitivities of these regional forcing experiments are again consistent with those for corresponding global aerosol forcings found in the literature. However, the regional responses and regional apparent hydrological sensitivities do not align with the corresponding global values. Through a holistic approach involving analysis of the energy budget combined with exploring changes in atmospheric dynamics, we provide a framework for explaining the global and regional precipitation responses to regional aerosol forcing.

Supplemental information related to this paper is available at the Journals Online website: https://doi.org/10.1175/JCLI-D-17-0439.s1.

Corresponding author: Apostolos Voulgarakis, a.voulgarakis@imperial.ac.uk

1. Introduction

Understanding the influence that humans have on the planet through their emissions of anthropogenic greenhouse gases (GHGs) and aerosols is an important part of tackling the climate change challenge. The impact of

these anthropogenic forcers on the hydrological cycle is one of the main topics in climate change research (e.g., Wu et al. 2013), since any changes to radiatively active constituents can mean changes in the patterns of rainfall, droughts, and storms, all of which affect the livelihoods of people and ecosystems.

In response to this pressing issue, precipitation changes due to external climate forcers have been explored extensively by the climate science community (e.g., Andrews et al. 2010; Ming et al. 2010; Kvalevåg et al. 2013). GHGs, the strongest and most homogeneously distributed of all climate forcers, warm the climate system, increase water vapor in the atmosphere (Held and Soden 2000), weaken large-scale circulation (Held and Soden 2006), and can cause dry regions to get drier and wet regions to get wetter (Liu and Allan 2013). The climate responses to GHG forcing in the above studies are relatively robust, particularly in the global mean. However, large uncertainties are associated with anthropogenic aerosol influences.

Unlike well-mixed GHGs (WMGHGs), which have a fairly uniform distribution across the globe, atmospheric aerosols are a complex mixture of short-lived liquid and solid particles of varying sizes and optical properties, which have an inhomogeneous distribution across the globe due to their short lifetimes. This means that their radiative and hydrological effects vary strongly both in time and space. Therefore, aerosol species such as sulfate and black carbon (BC) exert more complex influences on radiative forcing than WMGHGs (Hodnebrog et al. 2014; Baker et al. 2015; Stohl et al. 2015; Storelvmo et al. 2016), and even more so on precipitation (Ramanathan et al. 2001; Mahowald 2011). In general, BC tends to warm the climate and stabilize the atmosphere while sulfate tends to cool the climate (Ramanathan and Carmichael 2008; Bond et al. 2013). Aerosol–radiation interactions, which impact both the surface and the atmosphere, and aerosol–cloud interactions give rise to very complicated and diverse features in resulting radiative forcings as well as precipitation (Rosenfeld et al. 2008; Ming et al. 2010; Rosenfeld et al. 2014; Baker et al. 2015; Boucher 2015). According to the Intergovernmental Panel on Climate Change (IPCC) Fifth Assessment Report (AR5) (Boucher et al. 2013), the aerosol–cloud–precipitation interactions are among the largest uncertainties in climate forcing.

Aside from the global net cooling effect of aerosols (Myhre et al. 2013a; Ming et al. 2010; Wu et al. 2013) and their cloud microphysical effects (Lee 2011; Rosenfeld et al. 2014; Altaratz et al. 2014), regional effects of aerosols on atmospheric circulation are also important for understanding or predicting precipitation change (Allen and Sherwood 2011; Bollasina et al. 2011; Polson

et al. 2014; Hodnebrog et al. 2016). Precipitation responses to aerosol forcing on regional scales have been found to be stronger than those for carbon dioxide in some locations (Shindell et al. 2012; Richardson et al. 2016; Hodnebrog et al. 2016), but the magnitude and even the sign depend on the forcing location and type (Shindell et al. 2012; Kasoar et al. 2018). However, these findings still need to be verified by further studies because of the large uncertainties involved in the related modeling aspects, as evidenced by the wide discrepancies among aerosol-induced responses seen in previous studies (Baker et al. 2015; Wilcox et al. 2015; Kasoar et al. 2016). Further efforts on quantifying the hydrological impacts of aerosols on global and regional scales will be crucial for informing policy, given aerosols' expected importance and the rapid shifts in their regional emissions (Hoesly et al. 2018). Also, the diversity of types and amounts of aerosols, and of the underlying meteorological conditions in the different emission regions of the globe, suggests that there is a need for regionally focused perturbation experiments of aerosol forcing and investigation of resulting effects. In particular, such differences are very pronounced between Asia and Europe/North America for both past and future atmospheres (Takemura 2012). Reducing these uncertainties and understanding the physical mechanisms that link regional aerosol forcing to global and regional precipitation changes are of paramount importance.

The Precipitation Driver Response Model Intercomparison Project (PDRMIP) was brought about to understand the differences in the precipitation response to various climate forcers as simulated by climate models. Idealized experiments involving large increases in GHGs and aerosols were used as inputs to drive 10 state-of-the-art climate models (Samset et al. 2016; Myhre et al. 2017). Some initial studies have already been produced using the PDRMIP dataset, all focused on a set of experiments where concentrations of various constituents were perturbed globally. In Samset et al. (2016), global perturbation experiments investigating five climate forcers and involving nine models revealed that fast (i.e., within a few years) global precipitation responses due to atmospheric and land surface interactions scale with global mean atmospheric absorption, while slow (i.e., after several decades) global precipitation response driven by ocean–atmosphere interactions scales with global mean surface temperature, in agreement with some key previous studies (Andrews et al. 2010; Kvalevåg et al. 2013). Published PDRMIP results also show that rapid adjustments account for large regional differences in hydrological sensitivity across multiple global forcers (Myhre et al. 2017).

However, the fast and slow precipitation responses to regional forcing have been largely unexplored.

The present paper will analyze the precipitation response in three regional aerosol perturbation experiments that were performed in the framework of PDRMIP. PDRMIP offers a unique opportunity for elucidating the complexities of the aerosol effect on global and regional precipitation. The majority of multimodel studies so far have tended to take the perspective of global aerosol effects and simultaneously perturb all aerosol types (e.g., single-forcing experiments in CMIP5; Taylor et al. 2012). Other key studies have either only focused on the fast response through atmosphere-only simulations (Richardson et al. 2016), or have investigated only the total response through single-model coupled simulations (Shindell et al. 2012). PDRMIP presents a new dataset from a multimodel, multiconstituent, multiregion (Europe and Asia) perspective with both atmosphere-only and coupled simulations, a large undertaking never materialized in previous studies.

By analyzing the results, the generality of conclusions about the hydrological sensitivity as well as the fast and slow precipitation responses inferred in past studies from global perturbations is assessed (sections 3a to 3c). The local and remote responses to the aerosol forcings from Asia and Europe are analyzed, and the possible mechanisms driving the changes are explained. Moreover, energy budget calculations (section 3d) help enhance the understanding of the physical mechanisms involved (Muller and O'Gorman 2011; O'Gorman et al. 2012; Richardson et al. 2016). These are combined with an examination of circulation changes (section 3e) to provide a more complete understanding of energy and precipitation changes caused by the different forcers. Finally, agreements and discrepancies among the models are discussed (section 3f).

2. Methods

a. Models

Of the 10 models that contributed to PDRMIP, seven have performed the regional aerosol perturbation experiments analyzed here: GISS-E2, HadGEM3-GA4, IPSL-CM5A, MIROC-SPRINTARS (Spectral Radiation-Transport Model for Aerosol Species), CESM1-CAM4, CESM1-CAM5, and NorESM1 (Table 1; see https://www.ametsoc.org/PubsAcronymList for additional expansions of acronyms).

b. Experiments

Three regional perturbation experiments were conducted (also see Table 2): 1) present-day sulfate concentrations over Asia (10°–50°N, 60°–140°E) were

TABLE 1. Models used in the present study and their specifications.

Model	Version	Resolution (lon × lat)	Aerosol setup[a]	Indirect effects included[b]	References
HadGEM3	GA 4.0	1.875° × 1.25°, 85 levels	AeroCom Phase II concentrations	Sulfate: all indirect effects; BC: no indirect effects	Walters et al. (2014); Bellouin et al. (2011)
GISS	E2-R	2.5° × 2°, 40 levels	AeroCom Phase II concentrations	Sulfate and BC: No indirect effects	Schmidt et al. (2014); Menon et al. (2010); Koch et al. (2011)
NorESM1	NorESM1-M	2.5° × 1.9°, 26 levels	AeroCom Phase II concentrations	Sulfate and BC: All indirect effects	Bentsen et al. (2013); Iversen et al. (2013); Kirkevåg et al. (2013)
MIROC-SPRINTARS	5.9.0	1.4° × 1.4°, 40 levels	HTAP2 emissions (year 2010)	Sulfate and BC: All indirect effects	Watanabe et al. (2010); Takemura et al. (2009)
IPSL-CM	5A	3.75° × 1.9°, 19 levels	AeroCom Phase II concentrations	Sulfate and BC: First indirect effect	Dufresne et al. (2013); Szopa et al. (2013)
CESM1-CAM5		2.5° × 1.9°, 30 levels	CMIP5 Emissions (year 2005)	Sulfate and BC: All indirect effects	Hurrell et al. (2013); Kay et al. (2015)
CESM1-CAM4		2.5° × 1.9°, 26 levels	AeroCom Phase II concentrations	Sulfate and BC: No indirect effects	Gent et al. (2011); Neale et al. (2010)

[a] Information on the aerosol mixing state in different models can be found in Table 1 of Stjern et al. (2017). However, we note that here these will only be relevant for the emission-based models, as aerosol processing does not influence results in the concentration-based simulations.

[b] Refers to first and second indirect effects of aerosols perturbed, i.e., SO_4 and BC. Direct sulfate and BC effects and semidirect BC effects are included in all models.

TABLE 2. Model simulations analyzed in the current study. The scaling refers to concentrations, but in two models (MIROC-SPRINTARS and CESM1-CAM5) the corresponding anthropogenic emissions were increased by 10 times (see also Table 1).

Experiment	SULASIA	SULEUR	BCASIA	SO4 × 5	BC × 10
Specifications	SO_4 over Asia increased by 10 times	SO_4 over Europe increased by 10 times	BC over Asia increased by 10 times	SO_4 increased by 5 times globally	BC increased by 10 times globally

increased by a factor of 10 (experiment denoted as SULASIA), 2) present-day sulfate concentrations over Europe (35°–70°N, 10°–40°E) were increased by a factor of 10 (SULEUR), and 3) present-day black carbon concentrations over Asia were increased by a factor of 10 (BCASIA). All perturbations are introduced as step changes and perturbed concentrations are repeated each year in the simulation, with unperturbed aerosol concentrations remaining fixed at present-day levels in the control simulation. All responses are calculated by taking the difference between each perturbation simulation and the control simulation. For each model and experiment, a pair of simulations was performed: a fixed sea surface temperature simulation (called fSST) and a fully coupled atmosphere–ocean simulation (called "Coupled"). The fSST simulations were run for 15 years and the coupled simulations for 100 years. The concentrations of all nonaerosol anthropogenic forcers and natural forcers are kept at present-day levels (typically year 2000) in all the experiments, as are the SSTs for the fSST simulations. The regional experiments will also be compared to the core global aerosol perturbation PDRMIP experiments, that is, the SO4×5 and BC×10 simulations (Table 2) in which global sulfate and BC aerosols were scaled up by 5 and 10 times, respectively (Samset et al. 2016).

The SO_4 and BC aerosol concentrations used in the control experiment are multimodel mean monthly present-day concentrations (accounting both for anthropogenic and nonanthropogenic emissions) extracted from the submissions to AeroCom Phase II (see, e.g., Myhre et al. 2013b; Samset et al. 2013). Multimodel AeroCom means were used, calculated from 13 models for BC and from 5 models for sulfate. To form perturbations, they were multiplied by the stated factor, and both baseline and perturbed fields were regridded to the native resolution of each PDRMIP model. However, for some models it was not possible to perform simulations with prescribed concentrations (see Table 1). These models instead ran a baseline with present-day emissions and then multiplied anthropogenic emissions regionally by the prescribed factors of 10 (not necessarily producing exactly a tenfold increase in concentrations). We note that there is no particular tendency for the emissions-based models to produce a systematic

atmospheric aerosol burden bias compared to the concentration-based models in the simulations examined here. The resulting multimodel mean global aerosol burden changes as a consequence of these perturbations are 4.03 and $1.43 \, mg \, m^{-2}$ for SULASIA and SULEUR, correspondingly (compared to $10.95 \, mg \, m^2$ in the global $SO_4 \times 5$ perturbation), while the change in BCASIA is $0.48 \, mg \, m^{-2}$ (compared to $1.73 \, mg \, m^{-2}$ in the global BC×10 perturbation).

We note that while all models include direct aerosol effects of sulfate and BC as well as the semidirect effects of BC, there is a mixture of models including or not including aerosol indirect effects (AIEs) on clouds in the current simulations, or including only the first indirect effect (cloud albedo effect); see the fifth column of Table 1.

c. Analysis methods

Output from the last 10 years of the fSST simulations and the last 50 years of coupled simulations were used for the analysis, with the first 5 and 50 years of the fSST and coupled simulations, respectively, discarded as model spinup time. The multiannual means of temperature and precipitation were calculated, and the difference was taken from the control simulation. The corresponding variables were regridded to a 3.75° × 2° (longitude × latitude) resolution for consistency between all models.

As in Samset et al. (2016), we calculated the apparent hydrological sensitivity (AHS), as the total precipitation change per unit global surface temperature change, in the fully coupled simulations. We have also separated the precipitation response into its fast and slow components. We define the fast precipitation response due to rapid adjustments, ΔP_{fast}, as the response calculated from the fSST simulations. In the coupled simulations, as in past studies (e.g., Samset et al. 2016), we have assumed that the total response over the last 50 years, ΔP_{total}, is a linear combination of the fast response and a slow response driven by surface temperature change. Hence, the slow response can be calculated as

$$\Delta P_{slow} = \Delta P_{total} - \Delta P_{fast}. \qquad (1)$$

Effective radiative forcing at the top-of-atmosphere (RF_{TOA}) and the surface (RF_{surf}) was calculated for

each perturbation from the change in global mean radiative fluxes in the fSST simulations (Forster et al. 2016). We also calculated the net atmospheric absorption AA using

$$AA = RF_{TOA} - RF_{surf}. \tag{2}$$

As well as the global mean forcing, we also investigate regional changes in the energy budget of the atmospheric column. Following the method developed by Muller and O'Gorman (2011) and applied by Richardson et al. (2016) and Hodnebrog et al. (2016), precipitation is related to the diabatic cooling and the dry static energy flux divergence of the atmosphere in the area examined as follows:

$$L_c \Delta P = \Delta Q + \Delta H, \tag{3}$$

where L_c is the latent heat of condensation of water vapor, equal to $29 \, W \, m^{-2} \, mm^{-1}$ day; P is the surface precipitation flux, in $mm \, day^{-1}$; Q is the column-integrated diabatic cooling (excluding latent heating) as shown in Eq. (4); H is the column-integrated dry static energy flux divergence, which is calculated as the residual between $L_c P$ and Q, as in the studies mentioned above; and Δ denotes the difference between the perturbation and the control experiment. The value of ΔQ is calculated as

$$\Delta Q = \Delta LW + \Delta SW - \Delta SH, \tag{4}$$

where LW is the net longwave radiative cooling and SW is the net shortwave radiative cooling from the atmospheric column, such that the difference in LW + SW between the top of the atmosphere (TOA) and the surface is equal to AA; SH is the net upward sensible heat flux at the surface.

3. Results

a. Precipitation response

Figure 1 shows the total, fast, and slow precipitation responses to the regional aerosol perturbations. For SULASIA (upper panels), the total response in Asia and downwind regions over the Pacific is a very strong decrease of precipitation, while other regions around the world experience a mixture of decreases and increases. The fast response in Asia is composed of a negative response over land and a positive response over the adjoining ocean, while the slow response shows the opposite. As has been suggested in past studies exploring Asian responses to local aerosols in an atmosphere-only framework (Dong et al. 2016), the fast response over Asia is due to a weakening of monsoon circulations over

Asia related to the decreased land–ocean temperature contrast resulting from land cooling. The slow response is due to the gradual decrease in surface temperature, especially over the oceans (see Fig. 2 for the temperature change), and the displacement of the mean position of the ITCZ. The precipitation change over land in Asia is dominated by the fast response while all other regions are controlled by the slow response, suggesting that remote effects require ocean-mediated changes in order to be established. Across the Pacific, Atlantic, and Indian Ocean basins, the total response broadly shows a southward shift of the ITCZ. This is consistent with previously reported ITCZ responses to hemispherically asymmetric cooling from a Northern Hemisphere aerosol perturbation (e.g., Acosta Navarro et al. 2017; Allen et al. 2015; Haywood et al. 2013; Hwang et al. 2013; Kang et al. 2008; Kirkevåg et al. 2008), leading the ITCZ to shift away from the cooler hemisphere. There is also a hint of an equatorward shift of the midlatitude storm tracks over the Pacific and more weakly so over the Atlantic.

SULEUR (middle panels in Fig. 1) shows similar but much weaker responses than SULASIA globally. This is due to the much smaller atmospheric sulfate burden change in SULEUR compared to SULASIA (approximately one-third). Table 3 shows the "efficacies" (a concept more often used for global temperature, representing the response per unit forcing; Hansen et al. 2005) of the radiative forcings resulting from the different aerosol perturbations, as well as the responses per unit global atmospheric aerosol burden change. The responses per unit burden change are larger for SULEUR than for SULASIA, both for temperature and for precipitation by a similar relative amount. The forcing efficacy (response per unit forcing) of SULEUR is also larger than that of SULASIA. The relative strength of SULEUR compared to SULASIA in terms of responses per unit burden is higher than the relative strength of their corresponding efficacies (1.5 compared to 1.1 for temperature and 1.6 compared to 1.2 for precipitation), suggesting that even though both the translation of forcing to response and the translation of burden to forcing contribute to the fact that SULEUR has a stronger response per unit burden change, possibly the latter (translation of burden to forcing) is the dominant factor. Stronger responses to European compared to (East) Asian aerosols have recently also been found by Kasoar et al. (2018), and suggested to be caused by a saturation of aerosol–cloud interactions over East Asia, as well as greater climatological cloud cover masking the direct aerosol forcing over East Asia (see also discussion in section 3f on the role of AIEs). It is noteworthy that the temperature response per unit forcing for global or
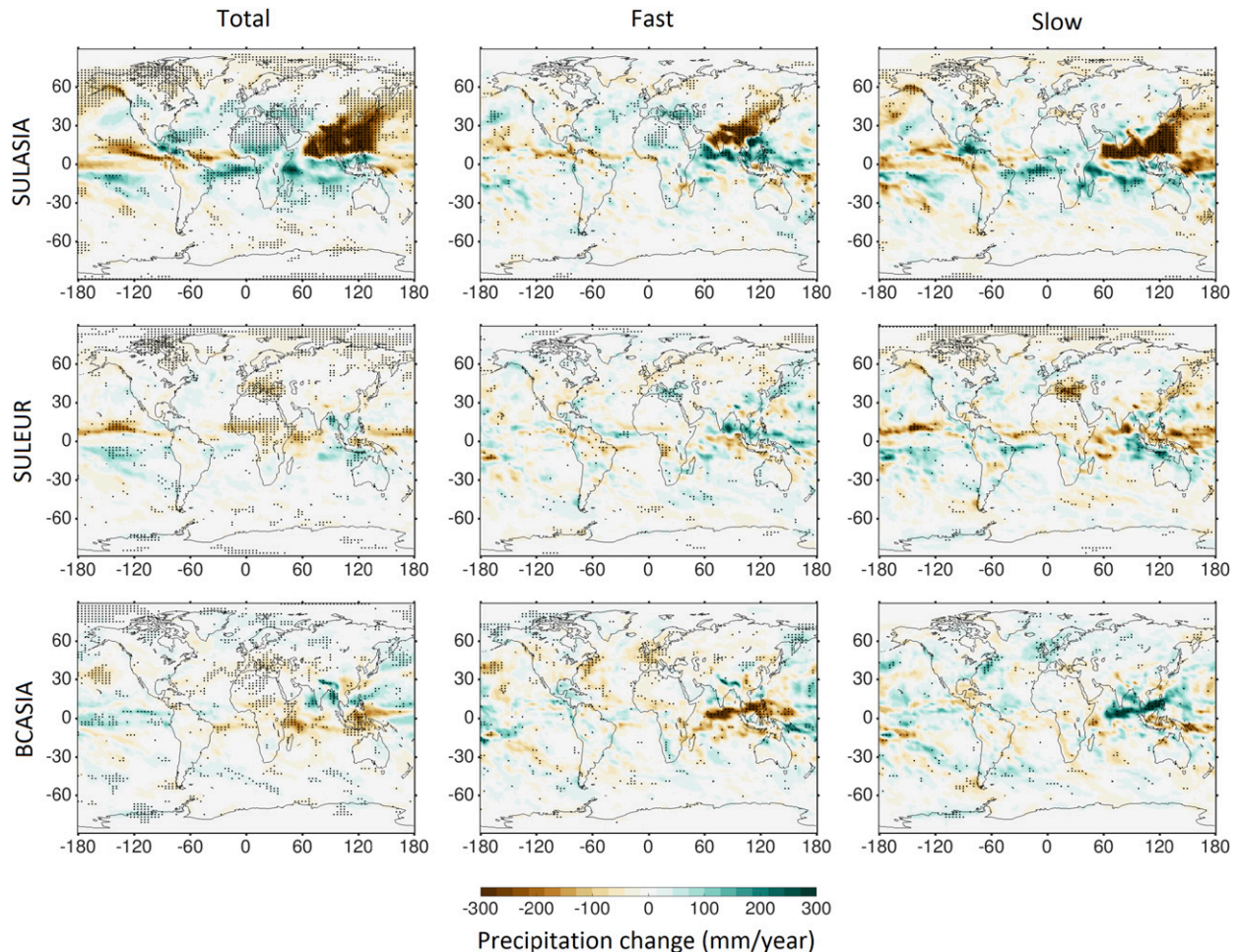
FIG. 1. Annual multimodel mean precipitation response in the regional aerosol perturbation experiments. The columns correspond to total, fast, and slow precipitation response, respectively. Stippled regions indicate where the multimodel mean precipitation change is at least one standard deviation away from zero.

regional sulfate perturbations is very similar to the response to doubled CO_2 [$\sim$0.55°–0.60°C $(W m^{-2})^{-1}$].

When it comes to the spatial pattern of responses in SULEUR, the change in ITCZ is similar to that in SULASIA but weaker. However, whereas in SULASIA the largest responses were seen around Asia itself, in SULEUR the precipitation responses around Europe are more modest, except for the significant precipitation reduction seen in the Mediterranean region. This feature is driven entirely by the slow responses, as in fact the fast responses are of opposite sign (i.e., precipitation increases). Still, it is the remote tropical responses that are the most pronounced in SULEUR. There is also a small but significant broad precipitation reduction over Arctic regions. The strong sensitivity of Arctic temperatures to European aerosol emissions has recently been highlighted by Acosta Navarro et al. (2016), and our results here hint toward something similar for

precipitation. All these features over Europe, the tropics, and the Arctic are dominated by the slow component.

For BCASIA (lower panels in Figs. 1 and 2), the responses in Asia are found to be uncertain (i.e., model dependent) and show a complex pattern without uniform changes over land and ocean, even in the fast response. Surface air temperature generally decreases over Asia in BCASIA fSST except over the Himalayan region (Fig. 2, bottom right). Because the vertical profile of BC in PDRMIP is weighted toward low altitudes (Myhre et al. 2017), the temperature increase in the Himalayan region would likely come from the advection of the warmer air heated by BC by solar absorption from South and East Asia over to the Himalayas (Ramanathan and Carmichael 2008). Generally, the total precipitation response over Asia bears some resemblance to both the fast and the slow response. The
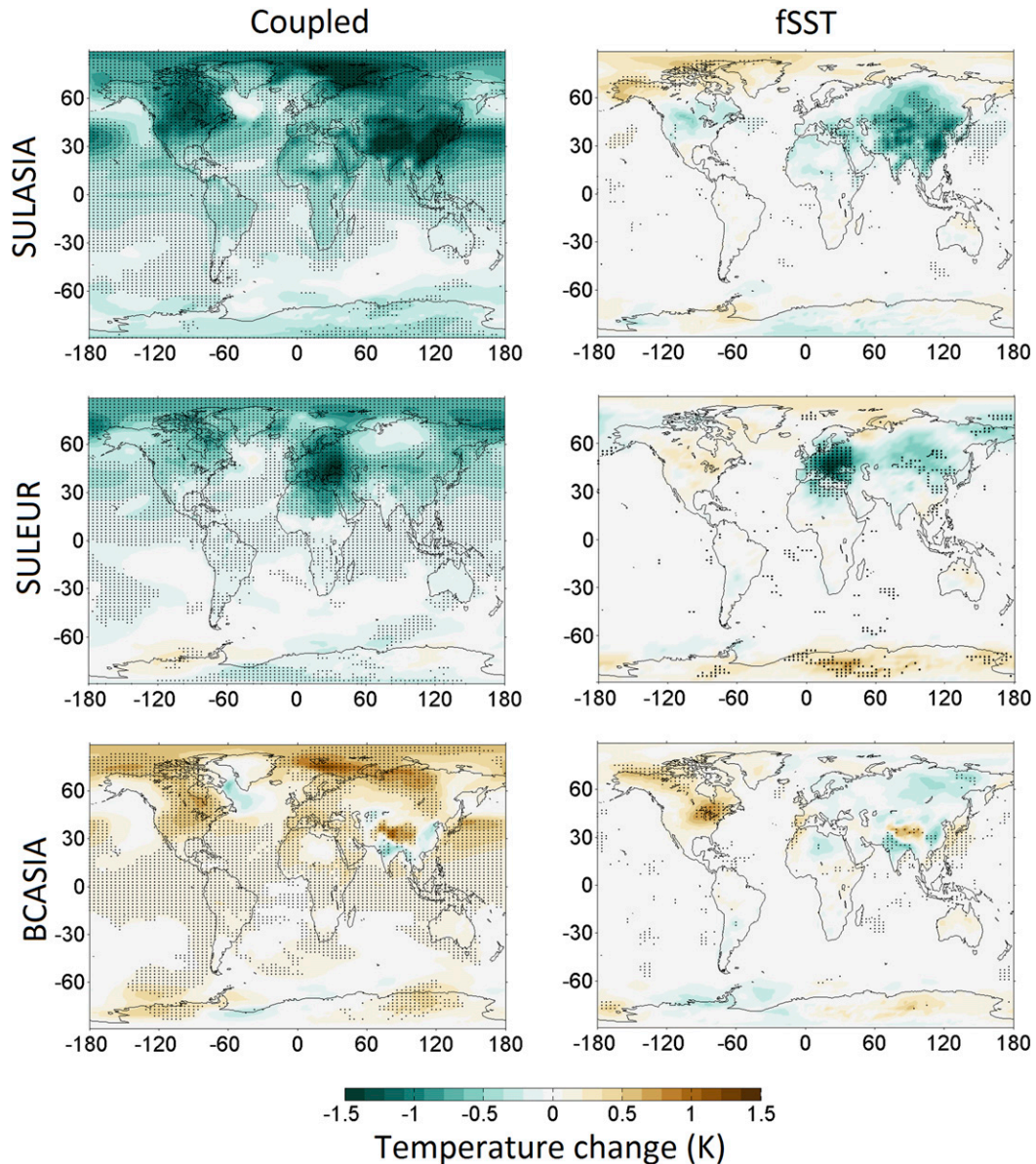
FIG. 2. Annual multimodel mean surface air temperature changes (K) in the regional experiments. Stippled regions indicate where the multimodel mean change departs from zero by more than one standard deviation.

positive precipitation increases over the Himalayas (Tibetan Plateau) are consistent with the mechanism proposed by past studies to dominate in the early parts of the monsoon season (Ramanathan and Carmichael 2008; Lau and Kim 2010; D'Errico et al. 2015), whereby the aforementioned solar heating enhances convection in the area, boosts the upper branch of the local Hadley circulation, and leads to stronger southwesterly flow and moisture fluxes into the region, subsequently driving the fast precipitation increases in this area. This mechanism appears to also dominate the total response (Fig. 1). Over East Asia, there is drying induced by Asian BC for

the southern parts of China and an increase in precipitation in the north, both being a result of fast adjustments. These southern decreases and northern increases of precipitation over China due to BC have also been found in other studies (Zhang et al. 2009), with the former attributed to the cooler land surface temperature reducing the surface thermal contrast that supports the East Asian summer monsoon circulation (Guo et al. 2013), and the latter attributed to upper-level circulation anomalies caused by the aforementioned heating of the Tibetan Plateau (Jiang et al. 2017). However, these East Asian responses are barely significant, not

TABLE 3. Efficacy of atmospheric concentration changes and of radiative forcings: Global mean temperature and precipitation responses per unit global aerosol burden change and per unit effective radiative forcing (ERF) in the different simulations (see Table 2).

	$\Delta T/\Delta$Burden (K mg^{-1} m^2)	$\Delta T/$ERF$_{TOA}$ (K W^{-1} m^2)	$\Delta P_{tot}/\Delta$Burden (% mg^{-1} m^2)	$\Delta P_{tot}/$ERF$_{TOA}$ (% W^{-1} m^2)
SO$_4 \times 5$[a]	-0.19 ± 0.15	0.57 ± 0.18	-0.55 ± 0.37	1.68 ± 0.54
SULASIA	-0.10 ± 0.04	0.58 ± 0.23	-0.25 ± 0.09	1.42 ± 0.54
SULEUR	-0.15 ± 0.08	0.66 ± 0.45	-0.39 ± 0.20	1.75 ± 1.11
BC $\times 10$[a]	0.27 ± 0.12	0.55 ± 0.29	-0.63 ± 0.56	-1.25 ± 1.18
BCASIA	0.32 ± 0.22	-0.14 ± 2.00	-0.51 ± 0.53	0.60 ± 5.60

[a] Calculated from the 7 models that also performed the regional simulations (see Table 1).

because there is no such feature (a dipole of negative changes in the south and positive ones in the north areas of East Asia) found in all the models, but because this dipole is actually found in somewhat different locations in the various models (see bottom row of Fig. S7, in the online supplemental material, referred to in section 3f). The total response over the Pacific and Indian Oceans in BCASIA shows some degree of northward shift in the ITCZ as it moves toward the Northern Hemisphere, which experiences widespread black carbon–induced heating.

The strength of global responses in BCASIA is generally much smaller than in SULASIA, in agreement with recent studies that also found sulfate to be a more important forcer of the global climate compared to BC (Baker et al. 2015). As was the case earlier when comparing SULEUR to SULASIA, this appears to be due to the much smaller mass of BC compared to sulfate in the atmosphere, resulting to a smaller burden change in BCASIA compared to SULASIA or SULEUR. The responses per unit burden change are actually larger for BCASIA, both for temperature and for precipitation (Table 3). As for sulfate (see above), the temperature response per unit forcing for the global BC perturbations is very similar to the response to doubled CO$_2$. The response per unit forcing of Asian BC (BCASIA) varies enormously between the models both for temperature and for precipitation, so that even the sign cannot be clearly diagnosed.

As expected, local responses over the perturbation regions are found to be very similar in the regional experiments to what they were in the global experiments (Samset et al. 2016); that is, Asian responses in SULASIA and BCASIA are very similar to those in the global sulfate and BC perturbation experiments, respectively. Over those regions, the climate forcers cause a fast response opposed by a slow response over the ocean, as they do in the global experiments. The shifts of ITCZ in the current experiments (i.e., southward in SULASIA and northward in BCASIA) are also qualitatively similar to those in the global experiments, though weaker.

One possible cause of cross-model diversity may be the fact that some models applied emissions perturbations instead of concentration perturbations, given that feedbacks between climate and chemistry/microphysics can impact atmospheric concentrations of aerosols (e.g., Randles et al. 2013; Allen et al. 2016). We examined how our results would look had there been five models (concentration based) in our analysis instead of seven. The analysis revealed somewhat stronger and significant responses in broader regions, although the main features of the geographical pattern of Fig. 1 (and Fig. 2 for temperature) remained similar. We show the resulting maps in Figs. S1 and S2.

b. Hydrological sensitivity

The global multimodel mean temperature changes in the regional experiments are -0.4 ± 0.1 K, -0.2 ± 0.1 K, and 0.1 ± 0.1 K for SULASIA, SULEUR, and BCASIA, while the global precipitation changes are $-1.0\% \pm 0.4\%$, $-0.5\% \pm 0.3\%$, and $-0.2\% \pm 0.2\%$, respectively (Fig. 3, left panels). As expected, the absolute values of the changes, though substantial, are much smaller than those in the global experiments (Samset et al. 2016), due to the regional forcings themselves being smaller. However, the global apparent hydrological sensitivity is $2.4\% \pm 0.5\%$ K^{-1} and $2.6\% \pm 0.6\%$ K^{-1} for SULASIA and SULEUR, which are in very good agreement with the AHS of $2.8\% \pm 0.4\%$ K^{-1} for the global SO$_4 \times 5$ experiment reported in Samset et al. (2016), as well as the values found from global perturbations in other studies (Andrews et al. 2010). The AHS for BCASIA is $-1.4\% \pm 1.5\%$ K^{-1}, which is smaller than the value from the global BC experiment [$-3.5\% \pm 3.0\%$ K^{-1} in Samset et al. (2016)], but within its uncertainty. However, note that the mean calculated from the global simulations of just the models that performed the regional simulations was exactly identical to that from the global BC experiment (i.e., $-3.5\% \pm 3.0\%$ K^{-1}). Also, the uncertainties in this case are of similar size to the signals.

Overall, these results imply that the global precipitation change simply scales with the global temperature change
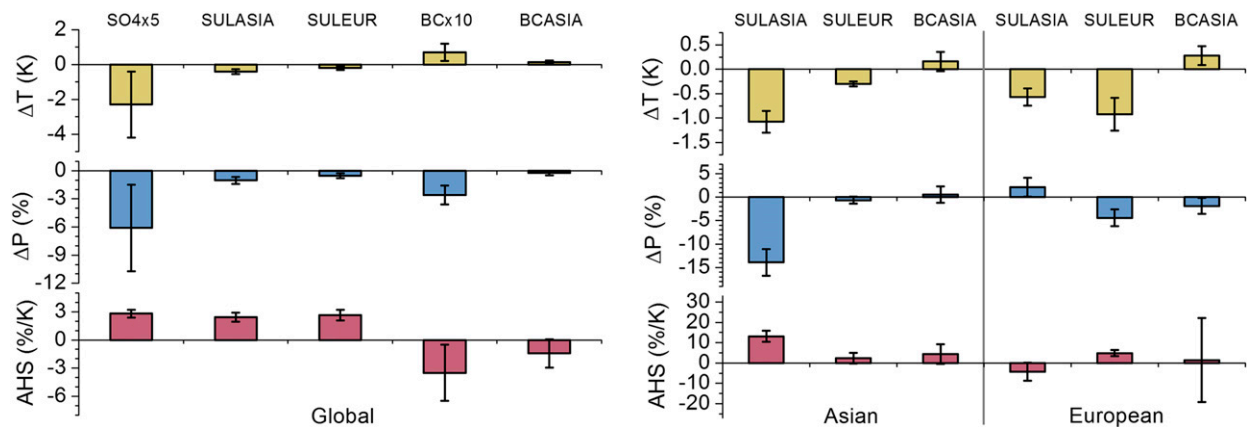
FIG. 3. (left) Global and (right) regional annual multimodel mean temperature change, precipitation change and apparent hydrological sensitivity (AHS) in the regional (SULASIA, SULEUR, BCASIA; performed by seven models) and global experiments [SO$_4$×5 and BC×10; performed by 9 models, from Samset et al. (2016)]. The error bars represent $\pm 1\sigma$ of the annual mean response across the models. The global AHS in BCASIA excludes the value from GISS ($-104\% \pm 1770\%$ K^{-1}) since it is very different from others, due to a too small global temperature response signal involved in the calculation (primarily caused by extreme cooling in the North Atlantic). The Asian AHS in BCASIA excludes the value from IPSL-CM5A ($66\% \pm 627\%$ K^{-1}) for the same reason.

in absolute terms, for any given forcing, whether global or regional. Furthermore, it suggests that the AHS inferred from global perturbations can likely be applied for estimating global precipitation impacts of regional forcings, when the associated global temperature change is known.

Similarly to the global AHS, we can define the regional AHS as the ratio of the regional precipitation response to the local temperature change. We show the regional AHS for two selected example regions, namely Asia and Europe (i.e., the regions where aerosols were perturbed) (Fig. 3, right panels). The Asian AHS inferred from SULASIA is much higher in absolute terms than the European AHS inferred from SULEUR, suggesting that Asia has stronger precipitation sensitivity to local temperature change compared to Europe. This implies that, although the globally averaged precipitation response scales with the long-term global temperature change, the strength of regional precipitation responses depends on other factors, potentially associated with induced anomalous circulation patterns (e.g., monsoon modifications) resulting from the various forcings. In other words, the AHS can be a useful metric for global responses but not for regional responses.

The uncertainties (relative to the response signal) of all responses for all regions in BCASIA are much larger than in SULASIA, with most of the responses including zero within 1σ. BC warms the climate in the long term but also stabilizes the atmospheric column by reducing shortwave radiation at the surface and warming the atmosphere aloft through shortwave absorption. This feature of BC that is sensitive to its vertical profile and the mountainous topography in Asia makes the

responses for BC more complex compared to those for sulfate, with both positive and negative temperature changes found over Asia in the multimodel mean in BCASIA (Fig. 2). Moreover, with the exception of temperature increases over the Himalayas and decreases over central India, these responses are much less consistent among the models compared to the uniform and consistent temperature changes found in SULASIA, which leads to even less agreement in precipitation responses (Figs. 1 and 3) and AHS (Fig. 3) in BCASIA. It is noteworthy that the AHS over Asia in BCASIA is of opposite sign to the global AHS in the same experiment. Note that there were a few models with extremely large AHS in the BCASIA experiment, which mainly stems from the very small values of temperature change in the denominator. These were excluded from the calculation of multimodel mean AHS in order to avoid artificially skewed results.

c. Predictors of precipitation response

Although AHS is a good measure for global precipitation response, it varies for different forcings (e.g., positive for sulfate but negative for BC, as shown in the left panel of Fig. 3). Globally, past studies (Andrews et al. 2010; Kvalevåg et al. 2013) have shown that the fast (fixed SST) precipitation response scales with atmospheric absorption. The left panel of Fig. 4 shows the fast precipitation response versus atmospheric absorption for the global mean, and over the Asian and European regions individually, for each regional perturbation experiment. The global means closely follow the line fitted with the five global experiments from Samset et al. (2016), although some intermodel diversity exists. The
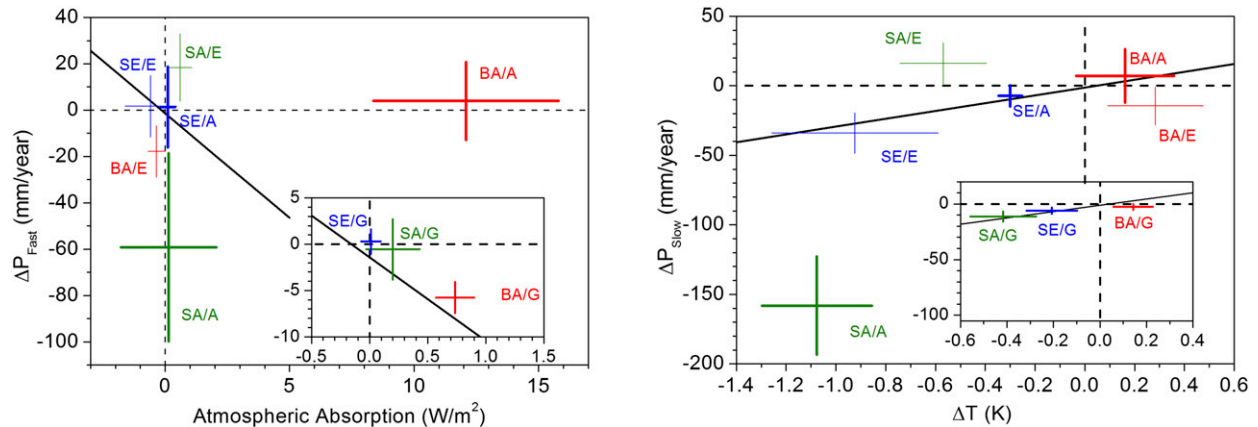
FIG. 4. (left) Regional and global fast annual multimodel mean precipitation responses vs global atmospheric absorption in the three regional aerosol perturbation cases, and (right) slow responses vs global temperature response. The black lines are the linear fits to the results from the five core global experiments in Samset et al. (2016) (with $R = -0.93$ for fast response and $R = 0.99$ for slow response). SA (green), SE (blue), and BA (red) represent SULASIA, SULEUR and BCASIA, respectively; /G, /A, and /E represent global, Asian, and European responses, respectively. The small (inner) frames also show the global responses, for perspective. The error bars represent $\pm 1\sigma$ of the multiyear annual mean response across the models.

regional responses have a wider range of ΔP_{Fast} for a given atmospheric absorption (crosses outside of the inner frames in Fig. 4 have a larger relative vertical extent compared to their horizontal extent). It is notable that the Asian response in SULASIA (SA/A) features the strongest negative fast precipitation response despite very little atmospheric absorption, while BCASIA (BA/A) features the strongest regional atmospheric absorption but with a small precipitation response. Generally for SULASIA and BCASIA the points on the graph (all SA and BA points) are far from the line fitted to the global values; the values for SULEUR (SE) are somewhat closer. Again, this implies that the local fast precipitation response may depend more on local dynamical adjustments than on simple large-scale thermodynamics.

Figure 4 (right panel) shows the global and regional slow precipitation response plotted against the global surface temperature response. As for the case of fast response, the global means closely follow the line by Samset et al. (2016). In contrast to what was found for fast response versus absorption, most of the regional responses also follow the line to some extent, implying that large-scale thermodynamic changes may play more of a role than the regional dynamics in driving the regional responses when long-term changes only are considered. The case that deviates drastically from this linear relationship is the response over Asia to local sulfate forcing in the SULASIA simulation (SA/A point), with a much stronger precipitation change per unit temperature change compared to the other cases. This suggests that possibly the synergy of both

large-scale effects (Northern Hemisphere temperature decreases shifting the ITCZ toward the south) and local effects (monsoon weakening due to a reduction of the land–sea thermal contrast over Asia) of Asian aerosols are at play and lead to this nonlinearity. A case that shows a particularly strong linear relationship that closely follows the global behavior is the Arctic, for which slow precipitation response plotted against temperature change for all the remote forcings sits very close to the line from Samset et al. (2016) representing the global forcings/responses (Fig. S3). The somewhat zonally uniform nature of this geographical region, which has less prominent topographical features than other areas of the globe examined, could potentially explain this fairly straightforward behavior.

We also explore the relationship of regional and global (total) precipitation responses with global TOA forcing in the three regional aerosol perturbation cases (Fig. 5). The global responses are found to follow a linear relationship with regional forcing (points within the inner frame), with SULASIA (SA/G) featuring both the strongest (negative) forcing and the strongest precipitation response (also negative). From the regional responses versus regional forcings (points outside the inner frame), first of all it can be seen that in all cases the local responses to a given forcing (SA/A, SE/E, BA/A) are the strongest, when compared to remote responses (SA/E, SE/A, BA/E), in agreement with recent findings by Kasoar et al. (2018). SULASIA shows a similar local response per unit local forcing [18.4 mm yr^{-1} (W m^{-2})$^{-1}$] to the global response per unit local (Asian) forcing [14.6 mm yr^{-1} (W m^{-2})$^{-1}$], while the corresponding
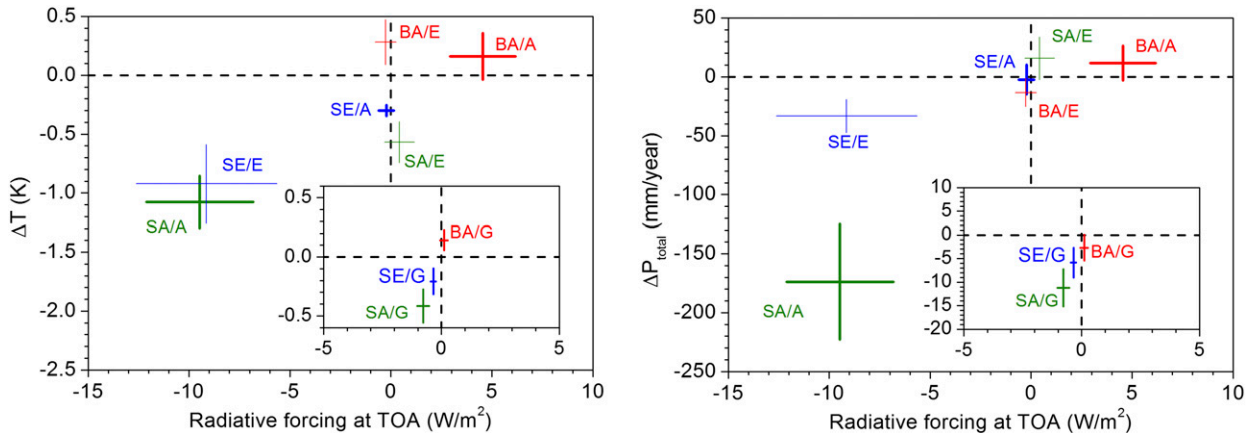
FIG. 5. Regional and global annual multimodel mean (left) temperature and (right) precipitation response plotted against global effective radiative forcing at TOA in the three regional aerosol perturbation cases. SA (green), SE (blue), and BA (red) represent SULASIA, SULEUR, and BCASIA, respectively; /G, /A, and /E represent global, Asian, and European responses, respectively. The small (inner) frames also show the global responses, for perspective. The error bars represent $\pm 1\sigma$ of the multiyear annual mean response across the models.

European value in SULEUR [3.6 mm yr^{-1} (W m^{-2})$^{-1}$] is much smaller than the global value [17.1 mm yr^{-1} (W m^{-2})$^{-1}$] (Fig. 5). The higher value in SULASIA than SULEUR again indicates that Asian precipitation is more sensitive to its local aerosol forcing than Europe, consistent with the AHS analysis above. Therefore, Asian sulfate is found to feature the strongest local precipitation change efficacy; despite having a forcing that is only marginally larger compared to that in the SULEUR simulation, and despite having a local temperature change efficacy that is very similar to that of SULEUR (left panel of Fig. 5), SULASIA causes a more than 5 times stronger precipitation response locally over Asia than SULEUR does over Europe. Still, as mentioned earlier, the efficacies of sulfate forcing from the two different regions for global precipitation are similar. Note that a similar conclusion is drawn also when using percentage precipitation changes instead of absolute, although in that case the Asian sulfate efficacy is 3 times larger instead of 5 times, compared to the European sulfate efficacy.

Figure S4 shows maps of precipitation responses per unit forcing. One key feature is that SULASIA and BCASIA have a similar pattern of negative precipitation efficacy over Europe (especially the Mediterranean), North Africa, and the Middle East, while SULEUR has a positive precipitation efficacy. Note that in the sulfate cases (SULASIA and SULEUR), the denominator of the calculation will be negative, which leads to a reversed sign compared to the absolute responses shown in Fig. 1. Effectively, what the first two panels of Fig. S4 show is the responses per unit of *positive* sulfate forcing [similar to the methodology in Shindell et al. (2012) or Hansen et al. (2005)], that is,

corresponding to a sulfur reduction and a heating over Asia, as in the case of BCASIA. The above-mentioned similarity in the response over Europe/North Africa/ the Middle East between SULASIA and BCASIA implies that forcing from either aerosol type over Asia may be affecting Europe via a similar mechanism, as opposed to forcing over Europe itself. Another similarity between SULASIA and BCASIA per unit forcing is a precipitation reduction across much of North America, which, however, is not a statistically significant feature, with the exception of a minority of grid points. Still, the most prominent feature is the shift of the ITCZ, which shows a more clear and similar pattern mainly in the sulfate perturbations (SULASIA and SULEUR).

d. Energy budget analysis

Figure 6 shows the energy budget analysis. Results show that, on a global scale, the energy of precipitation $L_c\Delta P$ is more likely to be governed by ΔQ (changes in column-integrated diabatic cooling; recall that this term does not include latent heating in our analysis) than by ΔH (changes in column-integrated dry static energy flux divergence), which is confirmed by examining the inner panel of the figure. The global average ΔH should be zero because it represents the energy transport due to the atmospheric circulation, which in the global mean is zero. In other words, the global latent heat energy of precipitation should balance with the net inward (outward) energy flux to (from) the atmosphere. Meanwhile, the energy budget analysis illuminates changes to the components of ΔQ. In the global mean, the breakdowns of the energy responses in SULASIA and SULEUR are very similar, while both are quite different from BCASIA.
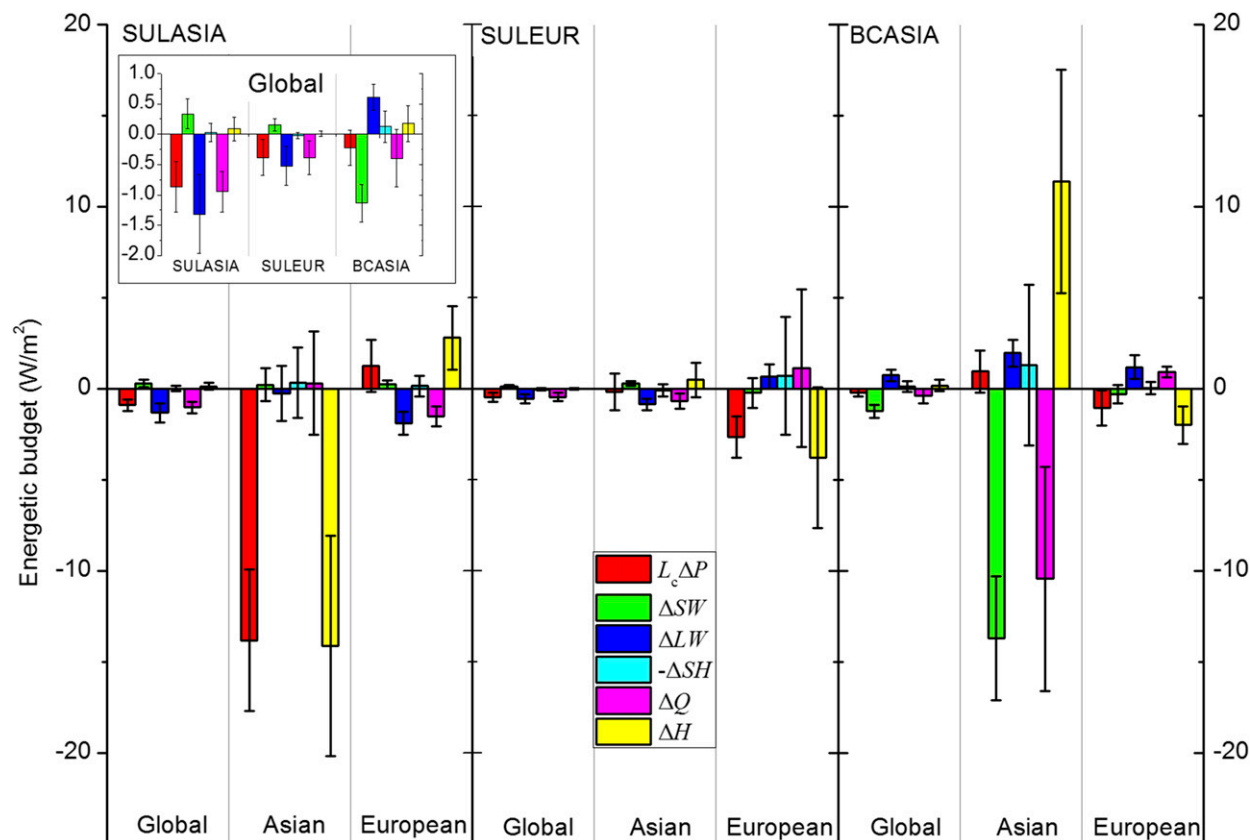
FIG. 6. The annual multimodel mean energy budget breakdown for the coupled simulations, showing changes in different source and sink terms of the atmospheric internal energy budget as in Eqs. (3) and (4), averaged globally and over the Asian and European perturbation regions for each experiment. It holds that $L_c\Delta P = \Delta Q + \Delta H$ [see Eq. (3) in section 2c], where $L_c\Delta P$ is the change in total latent heating; $\Delta Q = \Delta LW + \Delta SW - \Delta SH$ [Eq. (4)] is the change in net diabatic cooling of the atmospheric column due to shortwave and longwave radiation and sensible heat flux; and ΔH is the change in column-integrated dry static energy flux divergence. The inner frame shows the same values shown for the global column in the main figure, but with the scale range reduced for clarity. The error bars represent one standard deviation inferred from the different responses among the seven models.

The cooling of the atmosphere ΔQ depends on longwave radiative change in the sulfate experiments (driven by decreases in longwave emission due to surface cooling) whereas it depends on the shortwave in the BC experiment (driven by a decrease of shortwave radiation allowed to be reflected back to space).

Figure 6 also shows the changes in regional energy budgets for the European and Asian regions. The change in latent heating $L_c\Delta P$ in the regional means is generally much more consistent with ΔH rather than with ΔQ, indicating that, on regional scales, precipitation changes are closely tied to changes in the lateral transport of energy into and out of the column, and not to local radiative or sensible heat changes, consistent with findings for doubling of CO_2 (Richardson et al. 2016). The energy response over Asia in the BCASIA experiment shows somewhat different characteristics, with $L_c\Delta P$ being small despite a large increase in dry static energy flux divergence. The large ΔH term in

this region is compensating a large negative ΔQ term, which comes mainly from increased SW heating. The strong positive ΔH and weak positive ΔLW over Asia in response to BCASIA indicate that only a small amount of the heating due to BC absorption (green bar) is released locally as LW radiation (dark blue bar), and instead most of this heat is exported through the circulation (yellow bar). These results are qualitatively consistent with the analysis of Persad et al. (2017), who recently explored the influence of absorbing and scattering aerosols on the East Asian monsoon.

This demonstrates that changes in the export or import of energy are the preferred regional response to heating in the atmosphere. In the SULASIA and SULEUR experiments, as well as over Europe in the BCASIA experiment, there is no substantial change in atmospheric absorption, leading to the close relationship between $L_c\Delta P$ and ΔH. Over Asia in BCASIA, however, the large increase in SW absorption due to BC

becomes the dominant atmospheric heating term that must be balanced, and again this is done mainly by transport of heat rather than radiation. This regional picture is reversed in the global mean, however, because globally there can be no net export of heat through transport. The global energy budget in BCASIA therefore shows a relatively stronger LW response, such that it is now mostly LW radiative cooling that offsets the BC SW heating, along with a reduction in latent heating globally, that makes up for the rest of the difference. Globally, then, heat is discarded by LW radiation regardless of where the forcing is localized.

The preference for an atmospheric heating term to be balanced by energy divergence rather than diabatic cooling at regional scales is not limited to Asia and Europe: In the sulfate experiments, maps of the spatial distribution of each energy budget term (Fig. S5) show that ΔQ has only a small contribution to the changes in precipitation over almost all regions, whereas the patterns in $L_c \Delta P$ are almost identical to those in ΔH (i.e., regional precipitation is mostly controlled by the atmospheric dynamics across all parts of the world, whether locally to forcings or remotely). In BCASIA, ΔQ driven by shortwave absorption closely resembles the pattern of ΔH over Asia (but with opposite sign), while elsewhere the pattern of ΔH again resembles $L_c \Delta P$ (Fig. S5). The above is true both in the coupled and in the fixed SST simulations, which implies that the fast response is the dominant for BCASIA.

e. Role of atmospheric dynamics

We explore the atmospheric dynamical changes induced in the different experiments, to shed more light on the causes of precipitation changes. We focus on June–August (JJA), as this is the season of strongest impacts over monsoon-dominated regions, which are highly relevant for our study, as two out of three perturbations applied in our experiments are over Asia. In Fig. 7, when surface wind and sea level pressure changes (right panels) are compared to ΔH (left panels), one can easily conclude that the sea level pressure changes bear a strong resemblance to ΔH in Asia and Europe (i.e., the stronger ΔH is, the stronger the sea level pressure changes). The wind anomalies in SULASIA over East and South Asia are opposite in direction to the climatological monsoon flow in JJA, and the sea level pressure is higher than normal, both resulting from the lower temperatures caused by sulfate that lead to a weakened monsoon circulation. It is found that ΔH is strongly negative over Asia, indicating that more heat is converging over the region, which is in line with the monsoon circulation getting weaker, bringing less cooler air from above the oceans to above land. Dong et al. (2016)

also showed that both Asian and European sulfur dioxide emissions cause weakening of the East Asian summer monsoon (EASM) and therefore reduce East Asian precipitation, although in an atmosphere-only framework. The changes in surface wind direction moderate the monsoon circulation, which is largely responsible for precipitation in those regions. Similarly for Europe in SULEUR, the sea level pressure changes and weakening winds match up closely with the decrease in ΔH and therefore the decrease in precipitation.

In BCASIA, surface pressure over Asia decreases and the monsoon circulation is strengthened, but the effect is much weaker in magnitude compared to SULASIA (Fig. 7). The discrepancy between the seven models in BCASIA when it comes to the pressure change in Asia is large, so the net effect is not so robust in the multimodel mean, also reflected in the precipitation changes (Fig. 1).

Similar patterns of ΔH being in line with pressure and circulation changes are found even in remote regions. The most noteworthy feature is the significant and coherent decrease in ΔH over the southern parts of the North Atlantic and Europe in SULASIA, which is associated with induced cyclonic circulation and widespread decreases in pressure in that area. Simultaneously, pressure in high northern latitudes seems to be generally responding in a way that resembles the negative phase of the Arctic Oscillation (i.e., higher than normal pressures in the Arctic and lower than normal pressures farther south). Even more striking is the remote response in the Southern Hemisphere, which features a similar wavelike pattern in all the experiments, and, again, matches well the ΔH changes. This suggests the possible existence of an "interhemispheric teleconnection," whereby warming (cooling) the Northern Hemisphere causes both the intertropical convergence zone (ITCZ) and the Southern Hemispheric midlatitude jet to shift northward (southward) [Ceppi et al. 2013; also see Rotstayn et al. (2013) and Hwang et al. (2013)].

f. Discrepancies among the models

As shown above, we have drawn some robust conclusions from the multimodel mean behavior, but disagreements shall not be ignored. While examining the intermodel differences, one finds that locally the seven models are somewhat more consistent with each other in the coupled simulations than in the fSST simulations in the sulfate perturbation experiments, in terms of both the precipitation changes and the temperature changes (Figs. S6 and S7).

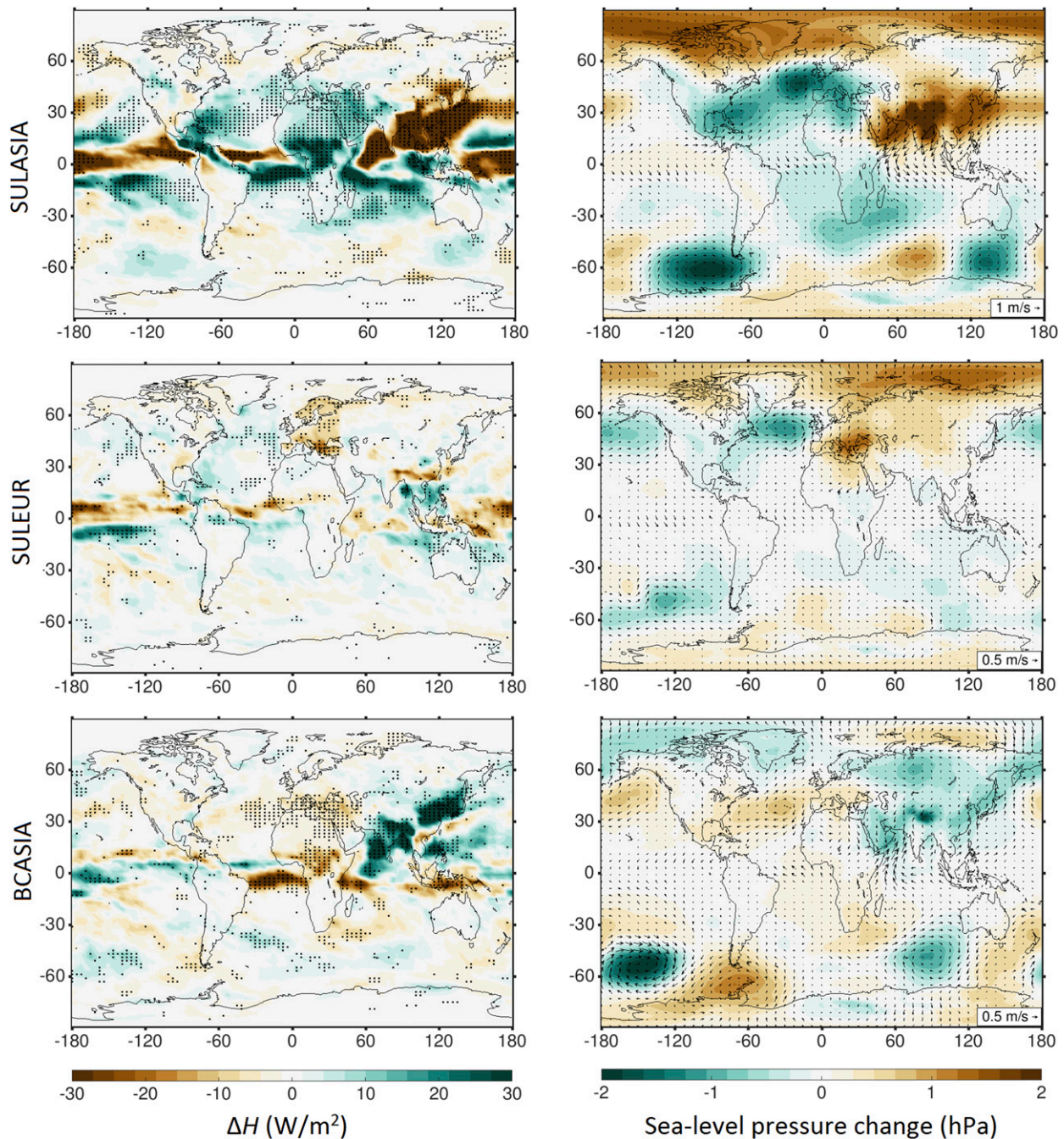The effect of sulfate on the atmosphere may be perceived as somewhat simpler compared to that of BC, and

FIG. 7. Comparison of June–August (JJA) (left) multimodel mean geographical changes in column-integrated dry static energy flux divergence (ΔH; in W m^{-2}) with (right) sea level pressure (hPa) and surface wind vector changes in the coupled simulations. Note that the color scales are opposite in terms of direction for ΔH and pressure.

this is beneficial when it comes to inferring robust simple relationships between forcing and response. However, as also discussed in other studies (Myhre et al. 2017; Kasoar et al. 2016), uncertainties still are substantial, even when ignoring uncertainties in the processes that translate emissions to concentration changes. It has to

be noted here that some of the multimodel range (error) could be a result of the fact that some models used prescribed emissions rather than concentrations in the simulations. However, as discussed in section 3a (discussion of Figs. S1 and S2), this does not appear to be the dominant driver of diversity.

In the case of BC, its influence is particularly uncertain even when considering its impacts on global mean precipitation (Pendergrass and Hartmann 2012). In BCASIA, the models may be broadly consistent in a qualitative sense when it comes to temperature change in most regions (Fig. 2), as well as when it comes to some of the most sizeable features of precipitation changes (Fig. 1), but especially over Asia even the geographical distribution of temperature changes varies particularly strongly across models, so that, for example, both strong positive and negative changes occur (Fig. S6; also see Fig. 2). The geographical distribution of precipitation changes shows an even more complex pattern and intermodel spread than temperature changes in BCASIA especially over Asia (Fig. S7; also see Fig. 1). The difference between the coupled and fSST runs suggest that the complete response involves strong modulation by the ocean, but also hints that land–atmosphere interactions, which are quite complex, are likely an important source of diversity between the models. Another point is that since aerosols are more concentrated in the lower atmosphere (Myhre et al. 2017), their distributions are affected strongly by the topography. This could contribute to differences in the geographical pattern of climate responses between models, especially in regions with complex topography such as the Himalayas, which implies a possible role of model resolution. However, HadGEM3 and MIROC-SPRINTARS are the highest resolution models among the ones used, and they do not show something particularly distinct in their temperature change characteristics. An additional possible reason for discrepancies especially for BC is that its precipitation effects largely depend on its vertical profile, which tends to vary largely between models (Ming et al. 2010; Ban Weiss et al. 2012; Pendergrass and Hartmann 2012; Samset et al. 2013; Hodnebrog et al. 2014).

Finally, there are differences in the way that the models handle the aerosol indirect effects on clouds—with some of them actually ignoring AIEs in the simulations presented here (Table 1)—and this could be perceived as a potential reason for diversity in climate responses (e.g., Kasoar et al. 2016). However, by examining the effective radiative forcing (ERF) over the aerosol perturbation regions (where AIEs would be expected to matter the most) in models that did not include AIEs (GISS, CESM1-CAM4) as compared to models that include all AIEs (HadGEM3, NorESM1, MIROC-SPRINTARS, CESM1-CAM5), we do not find any evidence of a strong role of AIEs in driving ERF diversity. GISS and CESM1-CAM4 produce ERF values of -11.9 and -10.3 W m^{-2}, respectively, over Asia in SULASIA, which are in fact higher than the average ERF from all the models (-9.5 W m^{-2}); for ERF over Europe in SULEUR, the corresponding values are -11.6 and -8.2 compared to an average of -9.2 W m^{-2}. Similarly, temperature and precipitation responses in models that include all AIEs and models that do not include any AIEs reveal no clear pattern for the former to produce stronger responses, and therefore AIE handling is likely of secondary importance in this case. The study of Wilcox et al. (2015) stressed the strong contribution of AIEs to CMIP5 model diversity when it comes to their simulated historical aerosol radiative forcing. But since here we are examining climate responses, there are additional factors at play, including climate sensitivity and changes in regional atmospheric dynamics. Furthermore, the sensitivity of cloud droplet number concentration to aerosol has been found to saturate at high aerosol concentrations (Carslaw et al. 2013). This implies that in the large perturbations examined here the magnitude of the AIE forcing may be converging between the different models that account for AIEs due to this saturation effect. However, since some of the models do not actually account for AIEs in the first place, this cannot be the full explanation of the lack of a strong role of AIEs in driving the diversity of climate responses between models.

Nevertheless, it is important to explore, constrain, and reduce uncertainty in model estimates of hydrological responses to regional aerosols in future studies.

4. Conclusions

Understanding the physical mechanisms behind precipitation responses to regional aerosol is of critical importance for being able to predict future climate, as well as to inform policy regarding the impacts of changing anthropogenic emissions from different regions. This study used seven models from the PDRMIP suite of simulations to explore the precipitation response to regional sulfate and black carbon (BC) aerosols. Crucially, the global apparent hydrological sensitivity (AHS) and the fast precipitation–atmospheric absorption and the slow precipitation–temperature relationships due to the regionally perturbed aerosols from Asia and Europe were found to be consistent with those from global sulfate and BC perturbation experiments from previous studies (Andrews et al. 2010; Kvalevåg et al. 2013; Samset et al. 2016). Therefore, the present results confirm that the previous findings of PDRMIP and other studies regarding global average precipitation responses hold for regional perturbations in the same way that they do for global. Also, we find that sulfate aerosols from Asia are a stronger driver of modeled global temperature and precipitation change compared to European aerosols, but

when the responses are normalized by unit radiative forcing or aerosol burden change, the picture reverses, with European aerosols being more efficient in driving global changes (i.e., having a higher global precipitation change "efficacy").

When it comes to local responses in the regions of the perturbations, Asian sulfate was found to be more effective per unit forcing in influencing precipitation locally (i.e., has a stronger local precipitation change efficacy) than European sulfate is for Europe. That is the case despite the fact that their temperature change efficacy is very similar. Asian precipitation is dominated by the monsoon system that itself is highly sensitive to localized forcings, and, as in previous studies, we found here that aerosols that scatter radiation have the impact of weakening the monsoon (Dong et al. 2016; Guo et al. 2016).

When it comes to nonlocal influences, both sulfate- and BC-induced forcings were found to drive precipitation responses remotely through influencing circulation, extending the influence of aerosols out of the emissions regions, and often to remarkably remote locations. There are some robust remote features of the precipitation responses, such as the shift of the ITCZ in all the experiments (i.e., southward in the sulfate increase experiments and northward in the BC increase experiment), the equatorward shift in the storm tracks in the Asian sulfate increase experiment, and the precipitation reduction over Europe (especially the Mediterranean) in the Asian BC increase experiment; the latter is currently being explored in detail in a separate PDRMIP study (Tang et al. 2017, manuscript submitted to *Atmos. Chem. Phys.*).

Analysis of the energy budget showed that the global average precipitation change depends mainly on the net atmospheric diabatic cooling (ΔQ), that is, the energy of precipitation $L_c \Delta P$ is consistently balanced by ΔQ on the global scale. Regionally, remote precipitation responses (i.e., responses outside of the perturbation region) were found to always be triggered by circulation changes. Regressions of fast precipitation response against atmospheric absorption and slow precipitation response against surface temperature change were proved to not be suitable for understanding regional responses, since they are not being applied to a closed system. On the regional scale, it is ΔH—which describes the changes in the energy transport by divergence and convergence of dry static energy (coming from influences in adjacent regions)—that is closely associated with regional precipitation responses.

We found that ΔH patterns correspond well to sea level pressure and wind change patterns, confirming the role of the dynamics in guiding the responses found. In the regions where the aerosols are perturbed, the sea level pressure

increases (decreases) following a cooling (warming) by sulfate (BC) aerosol, and the circulation diverges (converges), causing ΔH to decrease (increase) and therefore precipitation to decrease (increase) to balance the energy budget. The same arguments can be followed to explain the mechanisms associated with remote changes. Our approach therefore examines the full chain of processes involved in driving the precipitation responses to aerosols, is physically consistent with previous studies using energy budget analysis (Richardson et al. 2016) and circulation adjustment arguments (Shindell et al. 2012; Ming et al. 2011), and combines the two approaches to provide a holistic explanation of the mechanisms.

Overall, our study reveals that, in many ways, regional impacts of aerosols can be very different from their global impacts, suggesting that there is need for a deeper examination of how both atmospheric and oceanic dynamics translate a regional aerosol forcing to a local or a remote response and how real-world multiregional perturbations resulting from emissions play out. The fact that the responses are also to some extent dependent on the region of forcing and, especially for BC, on the model stresses the need for further coordinated studies in the future systematically investigating the impacts of different regional forcings (or emissions) of different species in multiple models. Also, it would be very informative to perform further multimodel simulations where concentrations have been scaled by different amounts, possibly smaller than the rather extreme perturbations applied here [e.g., apply 100% changes as in Kasoar et al. (2016, 2018)], in order to explore the linearity of responses both for temperature and for precipitation. Our study lays the path to improving climate model investigations of such responses and also helps to inform policy regarding local and remote pollution impacts on the hydrological cycle.

REFERENCES

Acosta Navarro, J. C., and Coauthors, 2016: Amplification of Arctic warming by past air pollution reductions in Europe. *Nat. Geosci.*, **9**, 277–281, https://doi.org/10.1038/ngeo2673.

——, and Coauthors, 2017: Future response of temperature and precipitation to reduced aerosol emissions as compared with increased greenhouse gas concentrations. *J. Climate*, **30**, 939–954, https://doi.org/10.1175/JCLI-D-16-0466.1.

Allen, R. J., and S. C. Sherwood, 2011: The impact of natural versus anthropogenic aerosols on atmospheric circulation in the Community Atmosphere Model. *Climate Dyn.*, **36**, 1959–1978, https://doi.org/10.1007/s00382-010-0898-8.

——, A. T. Evan, and B. B. Booth, 2015: Interhemispheric aerosol radiative forcing and tropical precipitation shifts during the late twentieth century. *J. Climate*, **28**, 8219–8246, https://doi.org/10.1175/JCLI-D-15-0148.1.

——, W. Landuyt, and S. Rumbold, 2016: An increase in aerosol burden and radiative effects in a warmer world. *Nat. Climate Change*, **6**, 269–274, https://doi.org/10.1038/nclimate2827.

Altaratz, O., I. Koren, L. A. Remer, and E. Hirsch, 2014: Review: Cloud invigoration by aerosols—Coupling between microphysics and dynamics. *Atmos. Res.*, **140–141**, 38–60, https://doi.org/10.1016/j.atmosres.2014.01.009.

Andrews, T., P. M. Forster, O. Boucher, N. Bellouin, and A. Jones, 2010: Precipitation, radiative forcing and global temperature change. *Geophys. Res. Lett.*, **37**, L14701, https://doi.org/10.1029/2010GL043991.

Baker, L. H., W. J. Collins, D. J. L. Olivié, R. Cherian, Ø. Hodnebrog, G. Myhre, and J. Quaas, 2015: Climate responses to anthropogenic emissions of short-lived climate pollutants. *Atmos. Chem. Phys.*, **15**, 8201–8216, https://doi.org/10.5194/acp-15-8201-2015.

Ban-Weiss, G. A., L. Cao, G. Bala, and K. Caldeira, 2012: Dependence of climate forcing and response on the altitude of black carbon aerosols. *Climate Dyn.*, **38**, 897–911, https://doi.org/10.1007/s00382-011-1052-y.

Bellouin, N., J. Rae, A. Jones, C. Johnson, J. Haywood, and O. Boucher, 2011: Aerosol forcing in the Climate Model Intercomparison Project (CMIP5) simulations by HadGEM2-ES and the role of ammonium nitrate. *J. Geophys. Res.*, **116**, D20206, https://doi.org/10.1029/2011JD016074.

Bentsen, M., and Coauthors, 2013: The Norwegian Earth System Model, NorESM1-M—Part 1: Description and basic evaluation of the physical climate. *Geosci. Model Dev.*, **6**, 687–720, https://doi.org/10.5194/gmd-6-687-2013.

Bollasina, M. A., Y. Ming, and V. Ramaswamy, 2011: Anthropogenic aerosols and the weakening of the South Asian summer monsoon. *Science*, **334**, 502–505, https://doi.org/10.1126/science.1204994.

Bond, T. C., and Coauthors, 2013: Bounding the role of black carbon in the climate system: A scientific assessment. *J. Geophys. Res. Atmos.*, **118**, 5380–5552, https://doi.org/10.1002/jgrd.50171.

Boucher, O., 2015: *Atmospheric Aerosols: Properties and Climate Impacts*. Springer, 311 pp.

——, and Coauthors, 2013: Clouds and aerosols. *Climate Change 2013: The Physical Science Basis*, T. F. Stocker et al., Eds., Cambridge University Press, 571–657.

Carslaw, K. S., and Coauthors, 2013: Large contribution of natural aerosols to uncertainty in indirect forcing. *Nature*, **503**, 67–71, https://doi.org/10.1038/nature12674.

Ceppi, P., Y.-T. Hwang, X. Liu, D. M. W. Frierson, and D. L. Hartmann, 2013: The relationship between the ITCZ and the Southern Hemispheric eddy-driven jet. *J. Geophys. Res. Atmos.*, **118**, 5136–5146, https://doi.org/10.1002/jgrd.50461.

D'Errico, M., C. Cagnazzo, P. G. Fogli, W. K. M. Lau, J. von Hardenberg, F. Fierli, and A. Cherchi, 2015: Indian monsoon and the elevated-heat-pump mechanism in a coupled aerosol–climate model. *J. Geophys. Res. Atmos.*, **120**, 8712–8723, https://doi.org/10.1002/2015JD023346.

Dong, B., R. T. Sutton, E. J. Highwood, and L. J. Wilcox, 2016: Preferred response of the East Asian summer monsoon to local and non-local anthropogenic sulphur dioxide emissions. *Climate Dyn.*, **46**, 1733–1751, https://doi.org/10.1007/s00382-015-2671-5.

Dufresne, J. L., and Coauthors, 2013: Climate change projections using the IPSL-CM5 Earth System Model: From CMIP3 to CMIP5. *Climate Dyn.*, **40**, 2123–2165, https://doi.org/10.1007/s00382-012-1636-1.

Forster, P. M., and Coauthors, 2016: Recommendations for diagnosing effective radiative forcing from climate models for CMIP6. *J. Geophys. Res. Atmos.*, **121**, 12 460–12 475, https://doi.org/10.1002/2016JD025320.

Gent, P. R., and Coauthors, 2011: The Community Climate System Model version 4. *J. Climate*, **24**, 4973–4991, https://doi.org/10.1175/2011JCLI4083.1.

Guo, L., E. J. Highwood, L. C. Shaffrey, and A. G. Turner, 2013: The effect of regional changes in anthropogenic aerosols on rainfall of the East Asian summer monsoon. *Atmos. Chem. Phys.*, **13**, 1521–1534, https://doi.org/10.5194/acp-13-1521-2013.

——, A. G. Turner, and E. J. Highwood, 2016: Local and remote impacts of aerosol species on Indian summer monsoon rainfall in a GCM. *J. Climate*, **29**, 6937–6955, https://doi.org/10.1175/JCLI-D-15-0728.1.

Hansen, J., and Coauthors, 2005: Efficacy of climate forcings. *J. Geophys. Res.*, **110**, D18104, https://doi.org/10.1029/2005JD005776.

Haywood, J. M., A. Jones, N. Bellouin, and D. Stephenson, 2013: Asymmetric forcing from stratospheric aerosols impacts Sahelian rainfall. *Nat. Climate Change*, **3**, 660–665, https://doi.org/10.1038/nclimate1857.

Held, I. M., and B. J. Soden, 2000: Water vapor feedback and global warming. *Annu. Rev. Energy Environ.*, **25**, 441–475, https://doi.org/10.1146/annurev.energy.25.1.441.

——, and ——, 2006: Robust responses of the hydrological cycle to global warming. *J. Climate*, **19**, 5686–5699, https://doi.org/10.1175/JCLI3990.1.

Hodnebrog, Ø., G. Myhre, and B. H. Samset, 2014: How shorter black carbon lifetime alters its climate effect. *Nat. Commun.*, **5**, 5065, https://doi.org/10.1038/ncomms6065.

——, ——, P. M. Forster, J. Sillmann, and B. H. Samset, 2016: Local biomass burning is a dominant cause of the observed precipitation reduction in southern Africa. *Nat. Commun.*, **7**, 11236, https://doi.org/10.1038/ncomms11236.

Hoesly, R. M., and Coauthors, 2018: Historical (1750–2014) anthropogenic emissions of reactive gases and aerosols from the Community Emission Data System (CEDS). *Geosci. Model Dev.*, **11**, 369–408, https://doi.org/10.5194/gmd-11-369-2018.

Hurrell, J. W., and Coauthors, 2013: The Community Earth System Model: A framework for collaborative research. *Bull. Amer. Meteor. Soc.*, **94**, 1339–1360, https://doi.org/10.1175/BAMS-D-12-00121.1.

Hwang, Y., D. M. W. Frierson, and S. M. Kang, 2013: Anthropogenic sulfate aerosol and the southward shift of tropical precipitation in the late 20th century. *Geophys. Res. Lett.*, **40**, 2845–2850, https://doi.org/10.1002/grl.50502.

Iversen, T., and Coauthors, 2013: The Norwegian Earth System Model, NorESM1-M—Part 2: Climate response and scenario projections. *Geosci. Model Dev.*, **6**, 389–415, https://doi.org/10.5194/gmd-6-389-2013.

Jiang, Y., and Coauthors, 2017: Anthropogenic aerosol effects on East Asian winter monsoon: The role of black carbon-induced Tibetan Plateau warming. *J. Geophys. Res. Atmos.*, **122**, 5883–5902, https://doi.org/10.1002/2016JD026237.

Kang, S. M., I. M. Held, D. M. W. Frierson, and M. Zhao, 2008: The response of the ITCZ to extratropical thermal forcing: Idealized slab-ocean experiments with a GCM. *J. Climate*, **21**, 3521–3532, https://doi.org/10.1175/2007JCLI2146.1.

Kasoar, M., A. Voulgarakis, J. F. Lamarque, D. T. Shindell, N. Bellouin, W. J. Collins, G. Faluvegi, and K. Tsigaridis, 2016: Regional and global temperature response to anthropogenic SO_2 emissions from China in three climate models. *Atmos. Chem. Phys.*, **16**, 9785–9804, https://doi.org/10.5194/acp-16-9785-2016.

——, D. Shawki, and A. Voulgarakis, 2018: Similar spatial patterns of global climate response to aerosols from different regions. *npj Climate Atmos. Sci.*, in press.

Kay, J. E., and Coauthors, 2015: The Community Earth System Model (CESM) Large Ensemble Project: A community resource for studying climate change in the presence of internal climate variability. *Bull. Amer. Meteor. Soc.*, **96**, 1333–1349, https://doi.org/10.1175/BAMS-D-13-00255.1.

Kirkevåg, A., T. Iversen, J. E. Kristjánsson, Ø. Seland, and J. B. Debernard, 2008: On the additivity of climate response to anthropogenic aerosols and CO_2, and the enhancement of future global warming by carbonaceous aerosols. *Tellus*, **60A**, 513–527, https://doi.org/10.1111/j.1600-0870.2008.00308.x.

——, and Coauthors, 2013: Aerosol–climate interactions in the Norwegian Earth System Model—NorESM1-M. *Geosci. Model Dev.*, **6**, 207–244, https://doi.org/10.5194/gmd-6-207-2013.

Koch, D., and et al, 2011: Coupled aerosol–chemistry–climate twentieth-century transient model investigation: Trends in short-lived species and climate responses. *J. Climate*, **24**, 2693–2714, https://doi.org/10.1175/2011JCLI3582.1.

Kvalevåg, M. M., B. H. Samset, and G. Myhre, 2013: Hydrological sensitivity to greenhouse gases and aerosols in a global climate model. *Geophys. Res. Lett.*, **40**, 1432–1438, https://doi.org/10.1002/grl.50318.

Lau, W. K. M., and K.-M. Kim, 2010: Fingerprinting the impacts of aerosols on long-term trends of the Indian summer monsoon regional rainfall. *Geophys. Res. Lett.*, **37**, L16705, https://doi.org/10.1029/2010GL043255.

Lee, S., 2011: Atmospheric science: Aerosols, clouds and climate. *Nat. Geosci.*, **4**, 826–827, https://doi.org/10.1038/ngeo1340.

Liu, C., and R. P. Allan, 2013: Observed and simulated precipitation responses in wet and dry regions 1850–2100. *Environ. Res. Lett.*, **8**, 034002, https://doi.org/10.1088/1748-9326/8/3/034002.

Mahowald, N., 2011: Aerosol indirect effect on biogeochemical cycles and climate. *Science*, **334**, 794–796, https://doi.org/10.1126/science.1207374.

Menon, S., D. Koch, G. Beig, S. Sahu, J. Fasullo, and D. Orlikowski, 2010: Black carbon aerosols and the third polar ice cap. *Atmos. Chem. Phys.*, **10**, 4559–4571, https://doi.org/10.5194/acp-10-4559-2010.

Ming, Y., V. Ramaswamy, and G. Persad, 2010: Two opposing effects of absorbing aerosols on global-mean precipitation. *Geophys. Res. Lett.*, **37**, L13701, https://doi.org/10.1029/2010GL042895.

——, ——, and G. Chen, 2011: A model investigation of aerosol-induced changes in boreal winter extratropical circulation. *J. Climate*, **24**, 6077–6091, https://doi.org/10.1175/2011JCLI4111.1.

Muller, C. J., and P. A. O'Gorman, 2011: An energetic perspective on the regional response of precipitation to climate change. *Nat. Climate Change*, **1**, 266–271, https://doi.org/10.1038/nclimate1169.

Myhre, G., and Coauthors, 2013a: Anthropogenic and natural radiative forcing. *Climate Change 2013: The Physical Science Basis*, T. F. Stocker et al., Eds., Cambridge University Press, 659–740.

——, and Coauthors, 2013b: Radiative forcing of the direct aerosol effect from AeroCom Phase II simulations. *Atmos. Chem. Phys.*, **13**, 1853–1877, https://doi.org/10.5194/acp-13-1853-2013.

——, and Coauthors, 2017: PDRMIP: A Precipitation Driver and Response Model Intercomparison Project—Protocol and preliminary results. *Bull. Amer. Meteor. Soc.*, **98**, 1185–1198, https://doi.org/10.1175/BAMS-D-16-0019.1.

Neale, R. B., and Coauthors, 2010: Description of the NCAR Community Atmosphere Model (CAM 4.0). NCAR Tech. Note NCAR/TN-485+STR, 212 pp., www.cesm.ucar.edu/models/ccsm4.0/cam/docs/description/cam4_desc.pdf.

O'Gorman, P. A., R. P. Allan, M. P. Byrne, and M. Previdi, 2012: Energetic constraints on precipitation under climate change. *Surv. Geophys.*, **33**, 585–608, https://doi.org/10.1007/s10712-011-9159-6.

Pendergrass, A. G., and D. L. Hartmann, 2012: Global-mean precipitation and black carbon in AR4 simulations. *Geophys. Res. Lett.*, **39**, L01703, https://doi.org/10.1029/2011GL050067.

Persad, G. G., D. J. Paynter, Y. Ming, and V. Ramaswamy, 2017: Competing atmospheric and surface-driven impacts of absorbing aerosols on the East Asian summertime climate. *J. Climate*, **30**, 8929–8949, https://doi.org/10.1175/JCLI-D-16-0860.1.

Polson, D., M. Bollasina, G. C. Hegerl, and L. J. Wilcox, 2014: Decreased monsoon precipitation in the Northern Hemisphere due to anthropogenic aerosols. *Geophys. Res. Lett.*, **41**, 6023–6029, https://doi.org/10.1002/2014GL060811.

Ramanathan, V., and G. Carmichael, 2008: Global and regional climate changes due to black carbon. *Nat. Geosci.*, **1**, 221–227, https://doi.org/10.1038/ngeo156.

——, P. J. Crutzen, J. T. Kiehl, and D. Rosenfeld, 2001: Aerosols, climate, and the hydrological cycle. *Science*, **294**, 2119–2125, https://doi.org/10.1126/science.1064034.

Randles, C. A., P. R. Colarco, and A. da Silva, 2013: Direct and semi-direct aerosol effects in the NASA GEOS-5 AGCM: Aerosol–climate interactions due to prognostic versus prescribed aerosols. *J. Geophys. Res. Atmos.*, **118**, 149–169, https://doi.org/10.1029/2012JD018388.

Richardson, T. B., P. M. Forster, T. Andrews, and D. J. Parker, 2016: Understanding the rapid precipitation response to CO_2 and aerosol forcing on a regional scale. *J. Climate*, **29**, 583–594, https://doi.org/10.1175/JCLI-D-15-0174.1.

Rosenfeld, D., U. Lohmann, G. B. Raga, C. D. O'Dowd, M. Kulmala, S. Fuzzi, A. Reissell, and M. O. Andreae, 2008: Flood or drought: How do aerosols affect precipitation? *Science*, **321**, 1309–1313, https://doi.org/10.1126/science.1160606.

——, S. Sherwood, R. Wood, and L. Donner, 2014: Climate effects of aerosol–cloud interactions. *Science*, **343**, 379–380, https://doi.org/10.1126/science.1247490.

Rotstayn, L. D., M. A. Collier, S. J. Jeffrey, J. Kidston, J. I. Syktus, and K. K. Wong, 2013: Anthropogenic effects on the subtropical jet in the Southern Hemisphere: Aerosols versus long-lived greenhouse gases. *Environ. Res. Lett.*, **8**, 014030, https://doi.org/10.1088/1748-9326/8/1/014030.

Samset, B. H., and Coauthors, 2013: Black carbon vertical profiles strongly affect its radiative forcing uncertainty. *Atmos. Chem. Phys.*, **13**, 2423–2434, https://doi.org/10.5194/acp-13-2423-2013.

——, and Coauthors, 2016: Fast and slow precipitation responses to individual climate forcers: A PDRMIP multimodel study. *Geophys. Res. Lett.*, **43**, 2782–2791, https://doi.org/10.1002/2016GL068064.

Schmidt, G. A., and Coauthors, 2014: Configuration and assessment of the GISS ModelE2 contributions to the CMIP5 archive. *J. Adv. Model. Earth Syst.*, **6**, 141–184, https://doi.org/10.1002/2013MS000265.

Shindell, D. T., A. Voulgarakis, G. Faluvegi, and G. Milly, 2012: Precipitation response to regional radiative forcing. *Atmos. Chem. Phys.*, **12**, 6969–6982, https://doi.org/10.5194/acp-12-6969-2012.

Stjern, C. W., and Coauthors, 2017: Rapid adjustments cause weak surface temperature response to increased black carbon concentrations. *J. Geophys. Res. Atmos.*, **122**, 11 462–11 481, https://doi.org/10.1002/2017JD027326.

Stohl, A., and Coauthors, 2015: Evaluating the climate and air quality impacts of short-lived pollutants. *Atmos. Chem. Phys.*, **15**, 10 529–10 566, https://doi.org/10.5194/acp-15-10529-2015.

Storelvmo, T., T. Leirvik, U. Lohmann, P. C. B. Phillips, and M. Wild, 2016: Disentangling greenhouse warming and aerosol cooling to reveal Earth's climate sensitivity. *Nat. Geosci.*, **9**, 286–289, https://doi.org/10.1038/ngeo2670.

Szopa, S., and Coauthors, 2013: Aerosol and ozone changes as forcing for climate evolution between 1850 and 2100. *Climate Dyn.*, **40**, 2223–2250, https://doi.org/10.1007/s00382-012-1408-y.

Takemura, T., 2012: Distributions and climate effects of atmospheric aerosols from the preindustrial era to 2100 along representative concentration pathways (RCPs) simulated using the global aerosol model SPRINTARS. *Atmos. Chem. Phys.*, **12**, 11 555–11 572, https://doi.org/10.5194/acp-12-11555-2012.

——, M. Egashira, K. Matsuzawa, H. Ichijo, R. O'Ishi, and A. Abe-Ouchi, 2009: A simulation of the global distribution and radiative forcing of soil dust aerosols at the Last Glacial Maximum. *Atmos. Chem. Phys.*, **9**, 3061–3073, https://doi.org/10.5194/acp-9-3061-2009.

Taylor, K. E., R. J. Stouffer, and G. A. Meehl, 2012: An overview of CMIP5 and the experiment design. *Bull. Amer. Meteor. Soc.*, **93**, 485–498, https://doi.org/10.1175/BAMS-D-11-00094.1.

Walters, D. N., and Coauthors, 2014: The Met Office Unified Model Global Atmosphere 4.0 and JULES Global Land 4.0 configurations. *Geosci. Model Dev.*, **7**, 361–386, https://doi.org/10.5194/gmd-7-361-2014.

Watanabe, M., and Coauthors, 2010: Improved climate simulation by MIROC5: Mean states, variability, and climate sensitivity. *J. Climate*, **23**, 6312–6335, https://doi.org/10.1175/2010JCLI3679.1.

Wilcox, L. J., E. J. Highwood, B. B. B. Booth, and K. S. Carslaw, 2015: Quantifying sources of inter-model diversity in the cloud albedo effect. *Geophys. Res. Lett.*, **42**, 1568–1575, https://doi.org/10.1002/2015GL063301.

Wu, P., N. Christidis, and P. Stott, 2013: Anthropogenic impact on Earth's hydrological cycle. *Nat. Climate Change*, **3**, 807–810, https://doi.org/10.1038/nclimate1932.

Zhang, H., Z. L. Wang, P. W. Guo, and Z. Z. Wang, 2009: A modeling study of the effects of direct radiative forcing due to carbonaceous aerosol on the climate in East Asia. *Adv. Atmos. Sci.*, **26**, 57–66, https://doi.org/10.1007/s00376-009-0057-5.